
Suzaku observations of two diffuse hard X-ray source regions, G22.0+0.0 and G23.5+0.1

Shigeo YAMAUCHI^{1,*}, Mayu SUMITA¹, and Aya BAMBA²

¹Department of Physics, Nara Women's University, Kitauoyanishimachi, Nara 630-8506

²Department of Physics and Mathematics, Aoyama Gakuin University,
5-10-1 Fuchinobe, Chuo-ku, Sagamihara, Kanagawa 252-5258

*E-mail: yamauchi@cc.nara-wu.ac.jp

Received ; Accepted

Abstract

G22.0+0.0 and G23.5+0.1 are diffuse hard X-ray sources discovered in the ASCA Galactic Plane Survey. We present Suzaku results of spectral analysis for these sources. G22.0+0.0 is confirmed to be a largely extended emission. The spectra were represented by a highly absorbed power-law model with a photon index of 1.7 ± 0.3 and a moderately absorbed thermal emission with a temperature of $0.34^{+0.11}_{-0.08}$ keV. The difference in the N_{H} values between the two components suggests that the thermal component is unrelated with the power-law component and is a foreground emission located in the same line-of-sight. G23.5+0.1 is an extended source with a size of $\sim 3'.5$. The spectra were fitted with an absorbed power-law model with a photon index of $2.4^{+0.5}_{-0.4}$. The spatial and spectral properties show that both are candidates of old pulsar wind nebulae (PWNe). In addition to the extended sources, we analyzed spectra of three point sources found in the observed fields. Based on the spectral features, we discuss origin of the sources.

Key words: ISM: supernova remnants — X-rays: individual (G22.0+0.0, G23.5+0.1) — X-rays: ISM — X-rays: stars

1 Introduction

Due to the large extinction, foreground radiation, and the contamination of nearby bright sources, it is difficult to detect faint sources located on the Galactic plane. Therefore, sample or information of the faint objects inside the Galactic plane has been limited. In the X-ray band above 3 keV, the interstellar medium is essentially transparent through the Galactic plane. Thus, observations in the hard X-ray band will be able to discover new faint X-ray sources on the Galactic plane. The ASCA satellite was the first satellite having an imaging capability up to 10 keV with an angular resolution of $\sim 3'$, expressed in terms of the half power diameter (HPD) (Tanaka et al. 1994). We carried out ASCA Galactic Plane Survey (AGPS) (Yamauchi et al. 2002) and detected many X-ray sources including unidentified sources (Sugizaki et al. 2001; Sakano et al. 2002).

G22.0+0.0 and G23.5+0.1 are hard X-ray sources discovered in the AGPS (Sugizaki et al. 2001; Ueno 2005; Ueno et al. 2006). The X-ray images showed that G22.0+0.0 has an extended emission with a radius of $\sim 5'$, while G23.5+0.1 has an arc-like structure (Ueno et al. 2006). The spectra were represented by an absorbed power-law (PL) model with a photon index $\Gamma=1.0^{+0.7}_{-0.3}$ and $N_{\text{H}} < 1.3 \times 10^{22} \text{ cm}^{-2}$ for G22.0+0.0 and $\Gamma=2.5^{+1.1}_{-0.8}$ and $N_{\text{H}}=(6^{+4}_{-3}) \times 10^{22} \text{ cm}^{-2}$ for G23.5+0.1 (90% confidence level) (Ueno 2005). A non-thermal supernova remnant (SNR) scenario was proposed (Ueno 2005; Ueno et al. 2006), but their nature was unsolved.

XMM-Newton, with a better angular resolution (half energy width $\sim 17''$ in orbit, XMM-Newton Users Handbook¹), observed the G23.5+0.1 region in a snapshot survey of plerionic and composite SNRs in the Galactic plane region in 2006 (Kargaltsev et al. 2012) and a follow up observation of SGR J1833–0832 in 2010 (Esposito et al. 2011). The observations clearly found an extended source around the radio pulsar B1830–08=PSR J1833–0827 ($P=85.3 \text{ ms}$, $\tau=P/2\dot{P}=147 \text{ kyr}$, $d=4.66 \text{ or } 5.7 \text{ kpc}$, Hobbs et al. 2004, 2005; Kargaltsev et al. 2012). The extended source is proposed to be a pulsar wind nebula (PWN) generated by B1830–08 (Esposito et al. 2011; Kargaltsev et al. 2012). The spectra of the whole source were fitted with an absorbed PL model with $\Gamma=2.3 \pm 0.8$ and $N_{\text{H}}=(3.9 \pm 1.9) \times 10^{22} \text{ cm}^{-2}$ (68% confidence level) (Kargaltsev et al. 2012), while the spectra of B1830–08 and the surrounding nebula were well represented by the absorbed PL model with Γ of $1.9^{+0.7}_{-0.6}$ and $1.7^{+0.5}_{-0.4}$ (68% confidence level), respectively (Esposito et al. 2011).

Since photon statistics in the ASCA and XMM-Newton observations were limited, their spectral parameters have large uncertainties. In order to reveal the spectral properties of the faint diffuse X-ray sources and to pin down their nature, the statistically good data are required. X-ray Imaging Spectrometers (XISs) onboard Suzaku has better spectral resolution and lower and more

¹ http://xmm.esac.esa.int/external/xmm_user_support/documentation/uhb/index.html

Table 1. Observation logs.

Field	Observation ID	Pointing Position	Observation time (UT)	Exposure
		$(\alpha, \delta)_{J2000.0}$	Start – End	(ks)
G22.0+0.0	505025010	(277° 8263, −9° 7167)	2010-04-16 14:27:26 – 2010-04-17 17:27:12	50.5
G23.5+0.1	505026010	(278° 4828, −8° 3633)	2010-10-20 13:34:39 – 2010-10-22 01:45:11	49.0

stable detector background than the previous X-ray satellites (Koyama et al. 2007; Mitsuda et al. 2007). Therefore, it is a suitable facility to study diffuse X-ray sources. We carried out follow up observations of G22.0+0.0 and G23.5+0.1 with Suzaku. Throughout this paper, the quoted errors are at the 90% confidence level.

2 Observations and data reduction

Suzaku observations of G22.0+0.0 and G23.5+0.1 were carried out with the XIS (Koyama et al. 2007) placed at the focal planes of the thin foil X-ray Telescopes (XRTs, Serlemitsos et al. 2007). The angular resolution (HPD) of the XRTs are 1'8–2'3 (Serlemitsos et al. 2007). The XIS is composed of 4 sensors. XIS 1 is a back-side illuminated (BI) CCD, while the other three XIS sensors (XIS 0, 2, and 3) are front-side illuminated (FI) CCDs. The field of view (FOV) of the XIS is 17'8×17'8. Since the XIS 2 stopped working on 2006 November 9, we used the data obtained with XIS 0, XIS 1, and XIS 3. A small fraction of the XIS 0 area was not used because of the data damage possibly due to an impact of micro-meteorite on 2009 June 23. The XIS was operated in the normal clocking mode with a time resolution of 8 s. The spectral resolution of the XIS was degraded due to the radiation of cosmic particles. In order to restore the XIS performance, the spaced-row charge injection (SCI) technique was applied. Details of the SCI technique are given in Nakajima et al. (2008) and Uchiyama et al. (2009).

Data reduction and analysis were made with the HEASoft version 6.16. The XIS pulse-height data for each X-ray event were converted to Pulse Invariant (PI) channels using the `xispi` software and the calibration database version 2014-07-01. We rejected the data acquired at the South Atlantic Anomaly, during the earth occultation, and at the low elevation angle from the earth rim of $< 5^\circ$ (night earth) and $< 20^\circ$ (day earth). After removing hot and flickering pixels, we used the grade 0, 2, 3, 4, and 6 data. The observation logs are listed in table 1.

3 Analysis and results

3.1 Image

Figure 1 shows X-ray images of the G22.0+0.0 and G23.5+0.1 fields in the 0.7–8 keV energy band. For maximizing the photon statistics, the data of XIS 0, 1, and 3 were added. In the G22.0+0.0 field, a largely extended emission with a diameter of $\sim 10'$ (hereafter Src1) is found at the FOV center, while in the G23.5+0.1 field, several sources are seen; three bright point-like sources at the north (hereafter Src3), near to the south edge (hereafter Src4), and at the center (hereafter Src5) and an extended source with a diameter of $\sim 3.5'$ at the southwest (hereafter Src2). Comparing the observed radial profile with the point-spread-function (PSF) simulated using `xissim`, we confirmed that Src1 and 2 have extents over the PSF and the others are likely to be point sources.

In addition, some faint sources are found in the images (for example, near to the southwest corner in the G22.0+0.0 field and northeast of Src5). Due to the limited photon statistics (the signal-to-noise ratio < 10), we were not able to determine their spectral parameters well. Therefore, we do not treat them in this paper.

The sky positions of Src1–5 are listed in table 2. For Src1 and Src2, we defined the brightest position in the Suzaku image as the source position. The typical positional uncertainty of Suzaku is $19''$ (Uchiyama et al. 2008), while the systematic error of the peak determination is $8''$.

The ASCA intensity map and the positions of XMM-Newton sources (3XMM DR4 version, Watson et al. 2009) are also shown in figure 1. All the sources have possible X-ray counterparts that were found in the previous observations. We found possible radio and optical counterparts for Src2 and Src3 (SIMBAD database), but no counterpart in the third Fermi Large Area Telescope source catalog (Acero et al. 2015). Using the NRAO VLA Sky Survey (NVSS) data (Condon et al. 1998), we also searched for extended radio emissions, but found no possible emission. The possible counterparts are listed in table 2.

3.2 Spectral analysis

Source spectra were extracted from the regions shown by the white solid lines in figure 1, while sky background data were taken from the source free regions in the same FOV, shown by the dotted lines. The source and the background regions were set to be common to XIS 0, 1, and 3. The region near the calibration source at the FOV corners and the damaged part of XIS 0 (north and south parts for G22.0+0.0 and G23.5+0.1 fields, respectively) were excluded. Response files, Redistribution Matrix Files (RMFs) and Ancillary Response Files (ARFs), were made using `xismfgen` and `xissimarfgen`, respectively. The non-X-ray background (NXB) for the source and the background

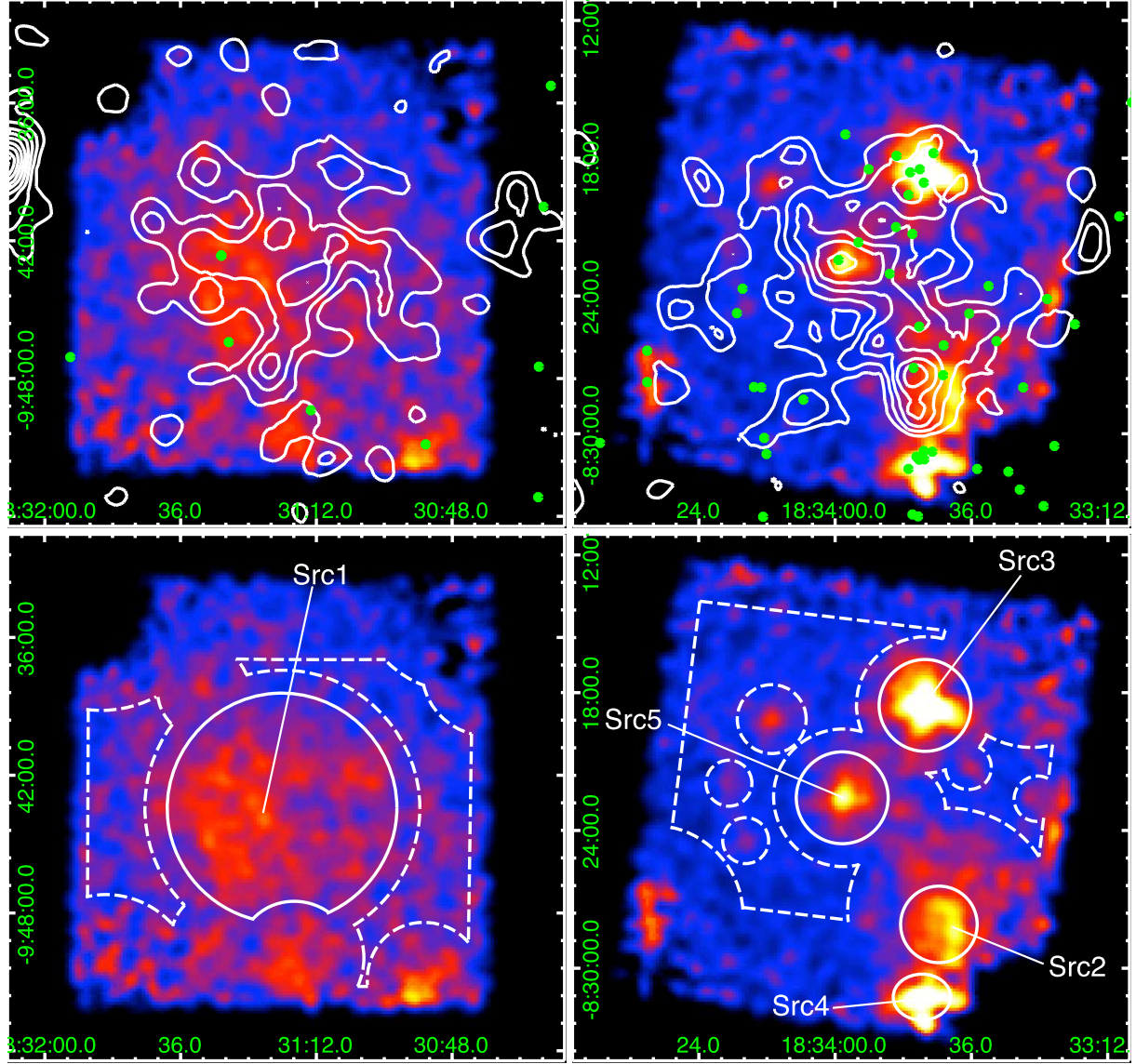


Fig. 1. Upper: XIS image of G22.0+0.0 (left) and G23.5+0.1 (right) fields obtained in the 0.7–8 keV band (color). The coordinates are J2000.0. The data of XIS 0, 1, and 3 were added. Background subtraction and vignetting correction are performed for the image. The intensity levels are linearly spaced. The green dots show the positions of X-ray sources in the XMM-Newton Serendipitous Source Catalog (3XMM DR4 version, Watson et al. 2009), while the white contours show the ASCA intensity map in the 0.7–8 keV band. Lower: the same XIS images as the upper panel (color). The white solid and dashed lines show source and background regions used for the spectral analysis, respectively.

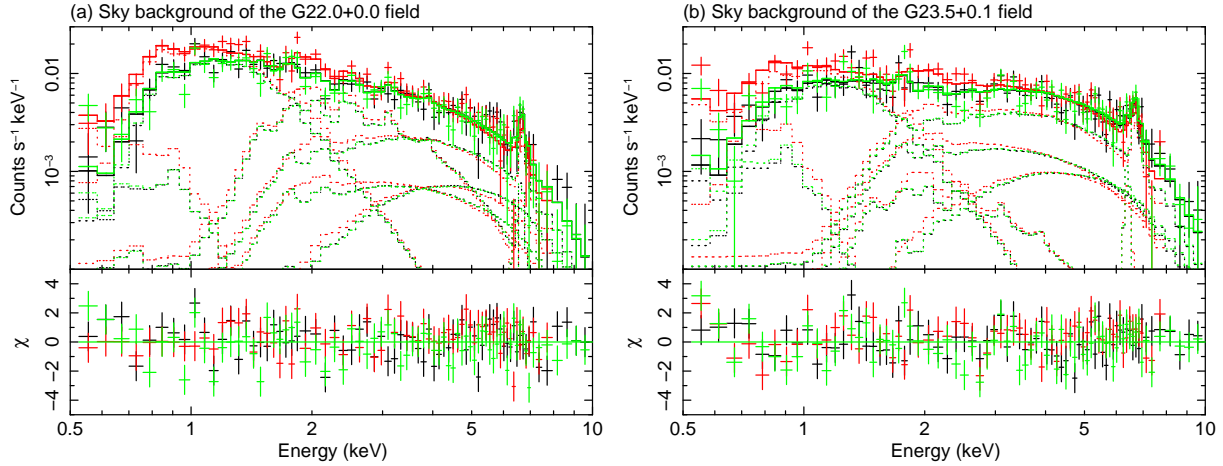


Fig. 2. NXB-subtracted background spectra of the G22.0+0.0 (a) and G23.5+0.1 (b) fields and the residuals from the best-fit models (see table 3). The XIS 0, 1, and 3 spectra were shown in black, red, and green, respectively. The dotted lines show each component.

spectra were extracted from the night-earth data (version 2014-06-01) using `xisnxbgen` (Tawa et al. 2008). The NXB was subtracted from the source and the background data.

3.2.1 Sky background estimation

Src1–5 are sources located on the Galactic plane, where a strong X-ray emission are found (e.g., Koyama et al. 1986). In order to minimize statistical uncertainty, we first evaluated sky background spectra and then modeled the sky background spectra with simulation.

The NXB-subtracted background spectra of the G22.0+0.0 and G23.5+0.1 fields are shown in figure 2. Uchiyama et al. (2013) reported that the blank sky spectra on the Galactic plane were well represented by a several component model as follows:

$$\begin{aligned}
 & [\text{TP}_1 (kT_e=0.09\text{keV}) + \text{TP}_2 (kT_e=0.59\text{keV})] \times \text{ABS1} + \\
 & [\text{TP}_L (kT_e=1.33\text{keV}) + \text{TP}_H (kT_e=6.64\text{keV}) + \text{RC}] \times \text{ABS2} + \\
 & \text{CXB} \times \text{ABS3}
 \end{aligned}$$

where TP, ABS, RC, and CXB show a thermal plasma model (`vapex` in XSPEC), photoelectric absorption (`phabs` in XSPEC, Balucinska-Church & McCammon 1992), a reflected component, and the Cosmic X-ray background. RC is composed of a PL function and $K\alpha$ (6.4 keV) and $K\beta$ (7.05 keV) lines from neutral Fe. The $K\beta$ line intensity was fixed to be $0.125 \times K\alpha$ line intensity (Kaastra & Mewe 1993) and the equivalent width of $K\alpha$ line was fixed to be 457 eV (Uchiyama et al. 2013). The metal abundances, temperatures, and the N_H value of ABS1 were fixed to those in Uchiyama et al. (2013) and the spectral parameters of the CXB were fixed to the values in Kushino et al. (2002). The N_H value of ABS3 is assumed to be twice of that of ABS2. Free parameters were normalizations of

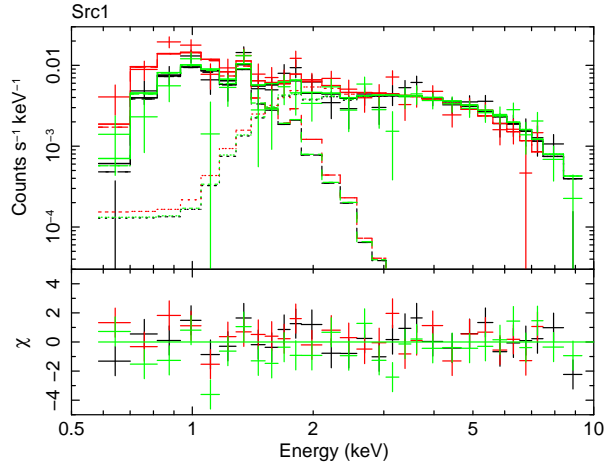


Fig. 3. XIS spectra of Src1 and the residuals from the best-fit $\text{PL} \times \text{ABS} + \text{TP} \times \text{ABS}$ model (see table 4). The XIS 0, 1, and 3 spectra were shown in black, red, and green, respectively. The dashed and the dotted lines show the TP and the PL models, respectively.

the TP models, the iron line intensity, and the N_{H} value of ABS2. The abundance tables were taken from Anders & Grevesse (1989), while the line and continuum data of the thin thermal plasma were taken from the ATOMDB v3.0.1. The XIS 0, 1, and 3 spectra were simultaneously fitted with the model. The model represented the spectra with reduced χ^2 ($\chi^2/\text{d.o.f.}$) values of 259.4/212=1.22 and 276.2/212=1.30 for the G22.0+0.0 and G23.5+0.1 fields, respectively. The best-fit model is plotted in figure 2, while the spectral parameters are listed in table 3. The surface brightness is consistent with those in Uchiyama et al. (2013). Using the best-fit parameters and assuming a 10^4 times longer exposure time, we simulated the sky background spectra for each source region and subtracted them from the NXB-subtracted source spectra.

3.2.2 G22.0+0.0 field

X-ray spectra of Src1 were extracted from a circle with a radius of $5'$. The background-subtracted spectra were displayed in figures 3. The spectra exhibit no significant emission line from S, and Fe and the TP model fit gave an extremely high temperature ($kT \sim 60$ keV). Thus, the thermal model is unlikely. The PL model fit gave a photon index and an N_{H} value of 0.95 and $<3 \times 10^{20} \text{ cm}^{-2}$, respectively, which are well consistent with the ASCA results (Ueno 2005). However, the reduced χ^2 was 152.4/82=1.86 and positive residuals were clearly seen below 1 keV. In addition, we see a weak line-like feature at 1.2–1.3 keV, which would be a K-line from Mg. Thus, we added a TP model (apec model in XSPEC) modified by low-energy absorption. The N_{H} values were set to be linked and the fit still gave a large reduced χ^2 value of 111.7/80=1.40. Next, the N_{H} values were set to be unlinked and then the fit was significantly improved ($\chi^2/\text{d.o.f.}=93.1/79=1.18$). The best-fit parameters are listed in table 4, while the best-fit model is plotted in figure 3.

3.2.3 G23.5+0.1 field

X-ray spectra of Src2, Src3, and Src5 were extracted from a circle with a radius of $100''$, $2'$, and $2'$, respectively, while those of Src4 were extracted from an ellipse with a size of $2'.5 \times 2'$. Since Src4 is located close to the calibration source of FIs and the damaged area of XIS 0, only the XIS 1 data were utilized. The background-subtracted spectra were shown in figure 4. The spectra were fitted with either the TP or the PL model modified by low-energy absorption. The best-fit parameters are listed in table 5 and the best-fit models are plotted in figure 4.

Applying the absorbed PL model for the Src5 spectra, we clearly found positive residuals at 6–7 keV, and hence we added an emission line with a line width of null. The $\Delta\chi^2$ value was 7.5, showing that the additional emission line model is at a 97 % confidence level. The center energy was determined to be $6.80^{+0.12}_{-0.07}$ keV, which indicates that the line is K-shell transition line from highly ionized iron. Thus, the emission from Src5 is thin thermal. An equivalent width (EW) was estimated to be 320 ± 200 eV.

4 Discussion

4.1 Extended sources

4.1.1 Src1

The spatial structure and the derived spectral parameters are very similar to the ASCA results (Ueno 2005; Ueno et al. 2006). Thus, Src1 is identified with AX J183114–0943. The spectra of Src1 are represented by two component model, the PL and TP model. The TP model is dominant below 1 keV (see figure 3), but no apparent source was found in the 0.7–1 keV band image. The N_{H} value of the TP model is about one-third of that of the PL model. These indicate that the thermal component is unrelated with the PL component and is a foreground emission located in the same line-of-sight. Here, we focus on the PL component.

The source region contains two XMM-Newton sources. The fluxes of 3XMM J183128.8–094239 and 3XMM J183127.5–094625 in the 0.2–12.0 keV energy band are 5.0×10^{-14} erg s $^{-1}$ cm $^{-2}$ and 9.5×10^{-14} erg s $^{-1}$ cm $^{-2}$, respectively (3XMM DR4 version). The flux of the PL component is estimated to be $\sim 10^{-12}$ erg s $^{-1}$ cm $^{-2}$ in the same energy band. Thus, we conclude that the contribution of XMM-Newton sources is small and most of X-rays ($\sim 85\%$) originate from the extended emission.

The Galactic HI column density (N_{HI}) along the line-of-sight to Src1 is $N_{\text{HI}} = 2.0 \times 10^{22}$ cm $^{-2}$ (Dickey & Lockman 1990) or $N_{\text{HI}} = 1.6 \times 10^{22}$ cm $^{-2}$ (Kalberla et al. 2005). The CO intensity at the source position (160–210 K km s $^{-1}$; Dame et al. 2001) and the conversion factor to the N_{H_2} value

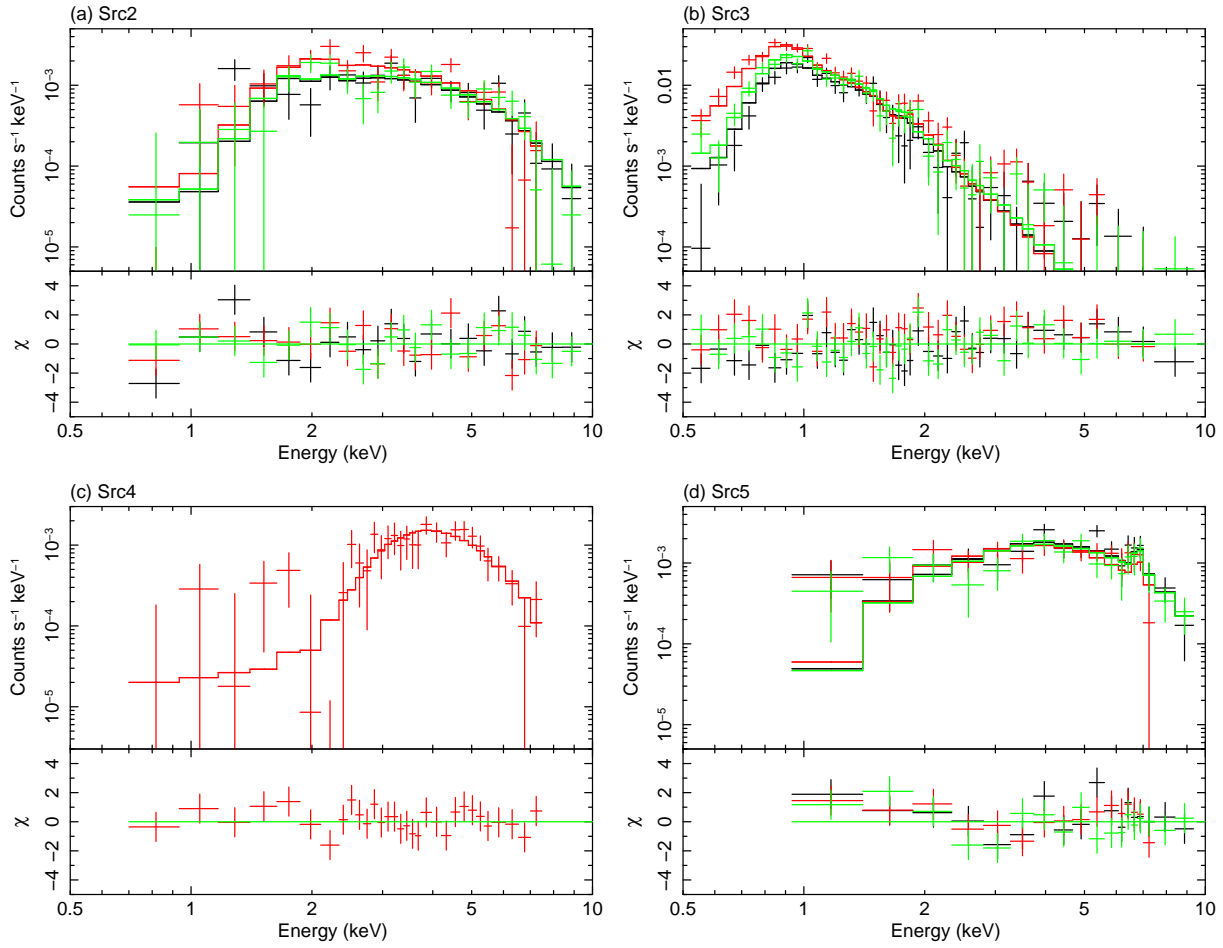


Fig. 4. XIS spectra of Src2 (a), Src3 (b), Src4 (c), and Src5 (d) and the residuals from the best-fit models: the PL model for Src2 and Src4 and the TP model for Src3 and Src5 (see table 5). The XIS 0, 1, and 3 spectra were shown in black, red, and green, respectively.

$[(1.8 \pm 0.3) \times 10^{20} \text{ cm}^{-2} \text{ K}^{-1} \text{ km}^{-1} \text{ s}]$; Dame et al. 2001] lead to the Galactic H_2 column density (N_{H_2}) of $(3.3 \pm 0.7) \times 10^{22} \text{ cm}^{-2}$. Thus, the total N_{H} , $N_{\text{H}} = N_{\text{HI}} + 2N_{\text{H}_2}$, is estimated to be $(8.4 \pm 1.4) \times 10^{22} \text{ cm}^{-2}$. The N_{H} value of Src1 is about 30 % of the total N_{H} through the Galaxy. If the line-of-sight length of the N_{HI} and N_{H_2} estimation in the radio band is assumed to be 17 kpc, double the distance from the Sun to the Galactic center, the distance of Src1 is $5.2 \pm 2.2 \text{ kpc}$.

The photon index of 1.7 ± 0.3 is typical values of PWNe ($\Gamma \sim 2$, e.g., Possenti et al. 2002; Kargaltsev & Pavlov 2008) rather than those of SN1006-like SNRs ($\Gamma \sim 2.5\text{--}3$, e.g., Koyama et al. 1995; Bamba et al. 2005). The X-ray image exhibits not shell-like but center-filled morphology. Thus, Src1 is likely to be a PWN. Taking account of the uncertainty of the distance, we estimated the X-ray luminosity in the 2–10 keV band and the angular size to be $(0.9\text{--}6.6) \times 10^{33} \text{ erg s}^{-1}$ and 9–22 pc, respectively. Possenti et al. (2002) and Mattana et al. (2009) presented the empirical relation between X-ray luminosity and the characteristic age of pulsars in PWNe. Bamba et al. (2010) showed the

relation between the characteristic age and the nebula size in the X-ray band. Comparing with the relations, we found that the estimated size and luminosity are consistent with those of PWNe with a larger characteristic age of $\sim 10^4$ – 10^5 yr.

Thus, all the facts support the idea that Src1 is a new candidate of an old PWN. However, we found no apparent high-energy compact source. To establish the scenario, search for the high-energy source is essential.

4.1.2 Src2

The source region contains a point source CXO J183340.3–082830=2MASS J18334038–0828304. The flux was estimated to be $\sim 7 \times 10^{-14}$ erg s $^{-1}$ cm $^{-2}$ in the 0.3–8 keV band (Chandra XAssist Source List, Ptak & Griffiths 2003), which is $\sim 16\%$ of the observed flux of Src2. The discrepancies of the flux and spatial structure indicate that CXO J183340.3–082830 is not a main counterpart of Src2. On the other hand, the spectral parameters of the PL model fit are fully consistent with those of source 8 in Kargaltsev et al. (2012), and are in agreement with those in Esposito et al. (2011) within the errors. Furthermore, the size is also consistent. Thus, these sources are identical.

Using $N_{\text{HI}}=2.1 \times 10^{22}$ cm $^{-2}$ (Dickey & Lockman 1990) or $N_{\text{HI}}=1.7 \times 10^{22}$ cm $^{-2}$ (Kalberla et al. 2005), the CO intensity at the source position of 180–230 K km s $^{-1}$ (Dame et al. 2001), we can estimate $N_{\text{H}}=(9.4 \pm 1.6) \times 10^{22}$ cm $^{-2}$ along the line-of-sight to Src2. The N_{H} value of $(3.5^{+1.1}_{-0.8}) \times 10^{22}$ cm $^{-2}$ of Src2 leads to the distance of 6.4 ± 2.3 kpc.

Src2 is a Galactic source with an extension of $\sim 3'$ – $4'$, suggesting an SNR or a PWN. If the X-rays have thermal origin, the higher temperature derived from the TP model fit suggests a young SNR such as Tycho and Kepler SNRs (e.g., Hwang, & Gotthelf 1997; Kinugasa, & Tsunemi 1999). However, we found no Si, S, and Fe emission lines that are typically seen in the SNR spectra; the abundance is very small (less than 0.24 solar, 90% confidence level). The photon index of $2.4^{+0.5}_{-0.4}$ is a typical value of SN 1006-like SNRs or PWNe (Possenti et al. 2002; Kargaltsev & Pavlov 2008; Koyama et al. 1995; Bamba et al. 2005). The X-ray luminosity in the 2–10 keV band and the size are estimated to be $(1.2\text{--}6.5) \times 10^{33}$ erg s $^{-1}$ and 4–9 pc, respectively. The angular size is small for a non-thermal SNR with the luminosity level (Nakamura et al. 2012). On the other hand, the observed properties of Src2 are well consistent with those of PWNe with the characteristic age of $\sim 10^4$ yr (Possenti et al. 2002; Mattana et al. 2009; Bamba et al. 2010). Thus, Src2 is likely to be an old PWN.

Esposito et al. (2011) and Kargaltsev et al. (2012) proposed that the extended nebula is a PWN generated by B1830–08=PSR J1833–0827. The estimated distance of Src2 is consistent with that of B1830–08, and hence our results support the scenario. Considering the characteristic age of B1830–08 ($\tau=147$ kyr), the size is a little bit small (Bamba et al. 2010). Some mechanisms to

prevent the nebula from expanding, such as interaction with SNR reverse shock (Gaensler & Slane 2006), may work or there may be a low surface brightness nebula that we have not found.

4.2 Point sources

4.2.1 Src3

Src3 exhibits softer spectra than the other sources. The TP model fit is acceptable (see table 5) and the spectral parameters are essentially the same as those in Kargaltsev et al. (2012).

Using the same method as those for Src1 and Src2, we can estimate the distance of Src3 to be 170 ± 100 pc, and hence the luminosity is calculated to be $(0.3\text{--}4.0) \times 10^{30}$ erg s $^{-1}$ in the 0.5–10 keV band. The spectral parameters and the luminosity are well consistent with those of late-type stars (e.g., Schmitt et al. 1990). Based on the SIMBAD database, B and V band magnitudes of BD-8 4632 (the optical counterpart of Src3) are 10.66 and 9.97, respectively. The observed N_{H} value and the empirical relation between N_{H} value and the color excess, E_{B-V} , of $N_{\text{H}}/E_{B-V} = (6.8 \pm 1.6) \times 10^{21}$ cm $^{-2}$ mag $^{-1}$ (Ryter et al. 1975) give the color, $B - V$, to be 0.55 ± 0.09 . These facts show that Src3 is a F–G type star. This is the same conclusion as that in Kargaltsev et al. (2012).

4.2.2 Src4

Src4 is most likely to be SGR J1833–0832 discovered on 2010 March 19 because the best-fit spectral parameters are in agreement with those of Göğüş et al. (2010) within the errors. The Suzaku observation was carried out on ~ 220 days after the outburst. The spectra of SGR J1833–0832 are well represented by an absorbed blackbody model (Göğüş et al. 2010; Esposito et al. 2011). Thus, we also applied the model and obtained the temperature of $0.83^{+0.23}_{-0.17}$ keV, the absorption column density of $(1.4^{+0.7}_{-0.5}) \times 10^{23}$ cm $^{-2}$, and the observed flux in the 2–10 keV of 6×10^{-13} erg s $^{-1}$ cm $^{-2}$ ($\chi^2/\text{d.o.f.} = 17.7/28$). Compared with the results in Göğüş et al. (2010) and Esposito et al. (2011), the temperature and the flux are gradually decreased after the Swift and XMM-Newton observations.

4.2.3 Src5

Src5 is identified with source 3 (=3XMM J183359.4–082226) in Kargaltsev et al. (2012). Kargaltsev et al. (2012) proposed that the source is either a neutron star binary (NSB), an active galactic nucleus (AGN), or a cataclysmic variable (CV). However, no spectral information on 3XMM J183359.4–082226 has been reported so far. The Suzaku observation revealed that the spectra are well represented by the TP model with a high temperature of > 10 keV and an weak Fe-K line at 6.8 keV ($EW = 320 \pm 200$ eV). These features are not found in NSB and AGN (e.g., White, Nagase, & Parmar 1995; Turner & Pounds 1989), but are well consistent with those of CVs (e.g., Ezuka &

Ishida 1999). The observed N_{H} value suggests the distance to be 7.9 ± 2.5 kpc. Then the luminosity in the 2–10 keV band is estimated to be $(1.9\text{--}6.9) \times 10^{33}$ erg s $^{-1}$, which is also in the range of CVs. Thus, all the facts indicate that Src5 is most likely to be a CV.

Acknowledgement

The authors are grateful to all members of the Suzaku team. This work was supported by JSPS KAKENHI Grant Number 24540232. This research has made use of the SIMBAD database, operated at CDS, Strasbourg, France.

References

- Acero, F., et al. 2015, ApJS, 218, 23
- Anders, E., & Grevesse, N. 1989, Geochim. Cosmochim. Acta, 53, 197
- Balucinska-Church, M., & McCammon, D. 1992, ApJ, 400, 699
- Bamba, A., Yamazaki, R., Yoshida, T., Terasawa, T., & Koyama, K. 2005, ApJ, 621, 793
- Bamba, A., Anada, T., Dotani, T., Mori, K., Yamazaki, R., Ebisawa, K., & Vink, J. 2010, ApJ, 719, L116
- Condon, J. J., Cotton, W. D., Greisen, E. W., Yin, Q. F., Perley, R. A., Taylor, G. B., & Broderick, J. J. 1998, AJ, 115, 1693
- Dame, T. M., Hartmann, Dap., & Thaddeus, P. 2001, ApJ, 547, 792
- Dickey, J. M., & Lockman, F. J. 1990, ARA&A, 28, 215
- Esposito, P., et al. 2011, MNRAS, 416, 205
- Ezuka, H., & Ishida, M. 1999, ApJS, 120, 277
- Gaensler, B. M., & Slane, P. O. 2006, ARA&A, 44, 17
- Göğüş, E., et al. 2010, ApJ, 718, 331
- Hobbs, G., Lyne, A. G., Kramer, M., Martin, C. E., & Jordan, C. 2004, MNRAS, 353, 1311
- Hobbs, G., Lorimer, D. R., Lyne, A. G., & Kramer, M. 2005, MNRAS, 360, 974
- Hwang, U., & Gotthelf, E. V. 1997, ApJ, 475, 665
- Kaastra, J. S., & Mewe, R. 1993, A&AS, 97, 443
- Kalberla, P. M. W., Burton, W. B., Hartmann, Dap, Arnal, E. M., Bajaja, E., Morras, R., & Pöppel, W. G. L. 2005, A&A, 440, 775
- Kargaltsev, O., & Pavlov, G. G. 2008, 40 years of Pulsars: Millisecond Pulsars, Magnetars and More, AIP conference proceedings Vol.983, 171
- Kargaltsev, O., Schmitt, B. M., Pavlov, G. G., & Misanovic, A. 2012, ApJ, 745, 99

- Kinugasa, K., & Tsunemi, H. 1999, PASJ, 51, 239
- Koyama, K., Makishima, K., Tanaka, Y., & Tsunemi, H. 1986, PASJ, 38, 121
- Koyama, K., Petre, R., Gotthelf, E. V., Hwang, U., Matsuura, M., Ozaki, M., & Holt, S. S. 1995, Nature, 378, 255
- Koyama, K., et al. 2007, PASJ, 59, S23
- Kushino, A., Ishisaki, Y., Morita, U., Yamasaki, N. Y., Ishida, M., Ohashi, T., & Ueda, Y. 2002, PASJ, 54, 327
- Mattana, F., et al. 2009, ApJ694, 12
- Mitsuda, K., et al. 2007, PASJ, 59, S1
- Nakajima, H., et al. 2008, PASJ, 60, S1
- Nakamura, R., Bamba, A., Dotani, T., Ishida, M., Yamazaki, R., & Kohri, K. 2012, ApJ, 746, 134
- Possenti, A., Cerutti, R., Colpi, M., & Mereghetti, S. 2002, A&A387, 993
- Ptak, A., & Griffiths, R. 2003, Astronomical Data Analysis Software and Systems XII, ASP Conference Series, Vol. 295, 465
- Ryter, C., Cezarsky, C., & Andouze, J. 1975, ApJ, 198, 103
- Sakano, M., Koyama, K., Murakami, H., Maeda, Y., & Yamauchi, S. 2002, ApJS, 138, 19
- Schmitt, J. H. M. M., Collura, A., Sciortino, S., Vaiana, G. S., Harnden, F. R. Jr., & Rosner, R. 1990, ApJ, 365, 704
- Serlemitsos, P., et al. 2007, PASJ, 59, S9
- Sugizaki, M., Mitsuda, K., Kaneda, H., Matsuzaki, K., Yamauchi, S. & Koyama, K. 2001, ApJS, 134, 77
- Tanaka Y., Inoue H., & Holt S. S. 1994, PASJ 46, L37
- Tawa, N., et al. 2008, PASJ, 60, S11
- Turner, T. J., & Pounds, K. A. 1989, MNRAS, 240, 833
- Uchiyama, H., et al. 2009, PASJ, 61, S9
- Uchiyama, H., Nobukawa, M., Tsuru, T. G., & Koyama, K. 2013, PASJ, 65, 19
- Uchiyama, Y., et al. 2008, PASJ, 60, S35
- Ueno, M. 2005, Ph.D. thesis, Kyoto University
- Ueno, M., Yamauchi, S., Bamba, A., Yamaguchi, H., Koyama, K., & Ebisawa, K. 2006, in proc. of IAU symposium 230, Populations of High Energy Sources in Galaxies, ed. E. J. A. Meurs & G. Fabbiano (Cambridge: Cambridge University Press), 333
- Watson, M. G., et al. 2009, A&A, 493, 339
- White, N. E., Nagase, F., & Parmar, A. N. 1995, in X-ray Binaries, ed. W. H. G. Lewin, J. van Paradijs, & E. P. J. van den Heuvel (Cambridge, Cambridge Univ. Press), Chapter 1
- Yamauchi, S., et al. 2002, in proc. of IAU 8th Asian-Pacific Regional Meeting Vol.II, ed. S. Ikeuchi, J. Hearnshaw, & T. Hanawa (Tokyo: ASJ), 81

Table 2. Source positions and possible counterparts.

ID	Name	Sky Position	Extent	Possible counterpart*	$\Delta\theta^\dagger$	References
Src	Suzaku J	(RA, Dec) _{J2000.0}			($''$)	
G22.0+0.0 field						
1	183121–0943	(18 ^h 31 ^m 21. ^s 5, −9°43′57 $''$)	Yes	AX J183114–0943 (X)	96	1
				3XMM J183128.8–094239 (X)	133	2
				3XMM J183127.5–094625 (X)	173	2
G23.5+0.1 field						
2	183339–0828	(18 ^h 33 ^m 39. ^s 1, −8°28′24 $''$)	Yes	CXO J183340.3–082830 (X)	19	3
				= 2MASS J18334038–0828304 (IR)	20	3
				3XMM J183341.0–082727 (X)	64	2
				= PSR B1830–08 (R)	56	3
				AX J183345–0828 (X)	104	1
3	183344–0818	(18 ^h 33 ^m 44. ^s 2, −8°18′32 $''$)	No	3XMM J183345.1–081829 (X)	14	2
				= SWIFT J183345.2–081831 (X)	15	3
				= BD-8 4632 (Opt)	16	3
				= 2MASS J18334527–0818294 (IR)	16	3
4	183344–0831	(18 ^h 33 ^m 44. ^s 7, −8°31′15 $''$)	No	CXO J183344.4–083108 (X)	9	3
				= 3XMM J183344.3–083107 (X)	10	2
				= SGR J1833–0832 (γ)	9	4
				3XMM J183345.2–083108 (X)	10	2
				3XMM J183345.7–083100 (X)	21	2
5	183358–0822	(18 ^h 33 ^m 58. ^s 8, −8°22′34 $''$)	No	CXO J183359.4–082229 (X)	11	3
				= 3XMM J183359.4–082226 (X)	12	2
				= AX J183356–0822 (X)	33	1

* X: X-ray, R: radio, IR: infrared, Opt: optical, and γ : γ -ray bands.

† Separation angle from the Suzaku position.

References: (1) Sugizaki et al. 2001; (2) XMM-Newton Serendipitous Source Catalog (3XMM DR4 version); (3) Simbad database; (4) Göğüş et al. 2010.

Table 3. The best-fit parameters of spectral analysis for the sky background.

Parameter	Value	
	G22.0+0.0 field	G23.5+0.1 field
$N_{\text{H},1}$ (cm^{-2})	5.6×10^{21} (fixed)	5.6×10^{21} (fixed)
$kT_{\text{e},1}$ (keV)	0.09 (fixed)	0.09 (fixed)
Norm* (TP ₁)	$(3.5 \pm 2.0) \times 10^{-3}$	$(5.0 \pm 1.8) \times 10^{-3}$
$kT_{\text{e},2}$ (keV)	0.59 (fixed)	0.59 (fixed)
Norm* (TP ₂)	$(4.6 \pm 0.3) \times 10^{-5}$	$(2.2 \pm 0.2) \times 10^{-5}$
$N_{\text{H},2}$ (cm^{-2})	$(3.8^{+0.4}_{-0.5}) \times 10^{22}$	$(3.2^{+0.6}_{-0.4}) \times 10^{22}$
$kT_{\text{e,L}}$ (keV)	1.33 (fixed)	1.33 (fixed)
Norm* (TP _L)	$(3.3 \pm 0.9) \times 10^{-5}$	$< 9.3 \times 10^{-6}$
$kT_{\text{e,H}}$ (keV)	6.64 (fixed)	6.64 (fixed)
Norm* (TP _H)	$(9.1^{+2.6}_{-2.7}) \times 10^{-6}$	$(1.2^{+0.3}_{-0.2}) \times 10^{-5}$
Z_{Ar}^{\dagger} (solar)	1.07 (fixed)	1.07 (fixed)
$Z_{\text{others}}^{\dagger}$ (solar)	0.81 (fixed)	0.81 (fixed)
Γ_{RC}	2.13 (fixed)	2.13 (fixed)
$I_{6.4\text{keV}}^{\ddagger}$	$(1.4 \pm 1.3) \times 10^{-8}$	$(2.4^{+1.3}_{-1.1}) \times 10^{-8}$
$N_{\text{H},3}$ (cm^{-2})	$= 2 \times N_{\text{H},2}$	$= 2 \times N_{\text{H},2}$
Γ_{CXB}	1.412 (fixed)	1.412 (fixed)
Norm [§] _{CXB}	8.2×10^{-7} (fixed)	8.2×10^{-7} (fixed)
$\chi^2/\text{d.o.f.}$	259.4/212	276.2/212

* Defined as $10^{-14} \times \int n_{\text{H}} n_{\text{e}} dV / (4\pi D^2)$, where n_{H} is the hydrogen density (cm^{-3}), n_{e} is the electron density (cm^{-3}), and D is the distance (cm). The unit is $\text{cm}^{-5} \text{ arcmin}^{-2}$.

[†] Relative to the solar value (Anders & Grevesse 1989).

[‡] The unit is photons $\text{s}^{-1} \text{ cm}^{-2} \text{ arcmin}^{-2}$.

[§] The unit is photons $\text{s}^{-1} \text{ cm}^{-2} \text{ keV}^{-1} \text{ arcmin}^{-2}$ at 1 keV.

Table 4. The best-fit parameters of spectral analysis for Src1 in the G22.0+0.0 field.

Parameter	Value		
Model	PL×ABS	(PL+TP)×ABS	PL×ABS+TP×ABS
N_H for PL ($\times 10^{22}$ cm $^{-2}$)	<0.03	$0.8^{+0.4}_{-0.2}$	$2.6^{+1.0}_{-0.9}$
Γ	$0.95^{+0.08}_{-0.09}$	$1.0^{+0.2}_{-0.1}$	1.7 ± 0.3
N_H for TP ($\times 10^{22}$ cm $^{-2}$)	—	0.8 (linked to N_H for PL)	$0.79^{+0.15}_{-0.13}$
kT_e (keV)	—	$0.28^{+0.09}_{-0.18}$	$0.34^{+0.11}_{-0.08}$
Abundance*	—	1.0 (fixed)	1.0 (fixed)
χ^2 /d.o.f.	152.4/82	111.7/80	93.1/79

* Relative to the solar value (Anders & Grevesse 1989).

Table 5. The best-fit parameters of spectral analysis for Src2–5 in the G23.5+0.1 field.

Parameter	Value							
	Src2		Src3		Src4		Src5	
Model	PL×ABS	TP×ABS	PL×ABS	TP×ABS	PL×ABS	TP×ABS	PL×ABS	TP×ABS
N_H ($\times 10^{22}$ cm $^{-2}$)	$3.5^{+1.1}_{-0.8}$	$2.9^{+0.7}_{-0.6}$	$0.45^{+0.08}_{-0.09}$	$0.09^{+0.06}_{-0.04}$	21^{+9}_{-7}	18^{+7}_{-5}	$2.5^{+1.9}_{-1.2}$	$5.1^{+1.4}_{-1.2}$
Γ / kT_e (keV)	$2.4^{+0.5}_{-0.4}$	$4.4^{+2.7}_{-1.3}$	$5.2^{+0.6}_{-0.5}$	$0.81^{+0.15}_{-0.05}$	$4.8^{+1.9}_{-1.4}$	$1.6^{+1.1}_{-0.6}$	0.9 ± 0.4	>10
Abundance*	—	<0.24	—	0.07 ± 0.02	—	<0.58	—	1.0 (fixed)
χ^2 /d.o.f.	78.3/62	76.3/61	242.4/122	138.5/121	18.2/28	17.9/27	53.2/49	51.5/49

* Relative to the solar value (Anders & Grevesse 1989).